

Using Landsat 8 and ASTER Data for lithological Discrimination and Mapping in Wadi Hamad area, North Eastern Desert, Egypt

Hassan Mohy¹, Fawzy F. Basta², Shaban Ghanem Saber³, Atef Fawzi Aziz El Sobky⁴

¹ Master degree and Unemployed but used to be Geologist in "National Authority for Remote Sensing and Space Sciences", ² Mineralogy and Petrology Geology Department, Faculty of Science Cairo University, Egypt.

³ Mineralogy and Petrology Geology Department, Faculty of Science, Beni-Suef University, Egypt

⁴ Master degree and Owner and Managing Director for "El; Sobky for Agencies, Import and Export"
atefelsobky@elsobkyceramic.com

Abstract: This research aims at exploring the potentiality of utilizing Landsat 8 in integration with the Advanced Spaceborne Thermal Emission and Reflection Radiometer (ASTER) data for lithological mapping of the Wadi Hamad area, North Eastern Desert of Egypt. Geological mapping in the Eastern Desert is impeded by difficult accessibility. By the use of Band combination, Principal Component Analysis (PCA) and Spectral ratioing of selected bands of Landsat 8 and ASTER data of the area, in synergy with geological field observation has proved effective in resolving geological mapping problems in the region. The validation mechanism was based on both matching interpreted lithological boundaries to the previously published geologic maps, field data and laboratory microscopic examinations of selected samples collected from the different exposed rocks in the area of study.

[Hassan Mohy Fawzy F. Basta, Shaban Ghanem Saber, Atef Fawzi Aziz El Sobky. **Using Landsat 8 and ASTER Data for lithological Discrimination and Mapping in Wadi Hamad area, North Eastern Desert, Egypt.** *J Am Sci* 2017;13(7):1-13]. ISSN 1545-1003 (print); ISSN 2375-7264 (online). <http://www.jofamericanscience.org>. 1. doi:[10.7537/marsjas130717.01](https://doi.org/10.7537/marsjas130717.01).

Keywords: ASTER; Landsat 8; Lithological mapping; Wadi Hamad area; Band ratio; Egypt.

1. Introduction

The Wadi Hamad area is located in the northern part of the Eastern Desert (ED) of Egypt. The ED constitutes the northern tip of the Arabian-Nubian Shield (ANS), which accreted following the collision of East and West Gondwana (Stern, 1994; Genna et al., 2002; Fritz et al., 2013). The ED is subdivided into South, Central and North provinces (Stern and Hedge, 1985). The ED is covered mainly by ophiolites and gneisses in the South province (SED), ophiolitic mélange and island arc volcano-sedimentary succession in the Central province (CED) and granitoids in the North province (NED).

The satellite data used in this study originates from two different multispectral imaging systems, which are frequently used for geological mapping through remote sensing, Landsat 8 and the Advanced Spaceborne Thermal Emission and Reflection Radiometer (ASTER). Landsat 8 covers the visible and near infrared (VNIR), short wave infrared (SWIR) and thermal infrared range (TIR) of the electromagnetic spectrum on 11 channels, including a deep blue coastal/aerosol band and a short-wave cirrus band. The resolution varies from 30 m for VNIR and SWIR (channels 1-7 and 9), 15 m for the panchromatic band 8, to 100 m for TIR (channel 10 and 11).

The Advanced Spaceborne Thermal Emission and Reflection Radiometer (ASTER) data are

collected in 14 bands, three in the visible and near-infrared (VNIR) portion of the electromagnetic spectrum with 15 m spatial resolution, six in the short-wave infrared (SWIR) with 30 m spatial resolution, and five in the thermal infrared (TIR) with 90 m spatial resolution. An advantage of ASTER data is the unique combination of wide spectral coverage and high spatial resolution in the visible near-infrared through shortwave infrared to the thermal infrared regions. The main objective of this study is to examine whether a combination of ASTER and Landsat 8 data exceeds the efficiency in mapping the lithological units in arid desert areas (e.g. Wadi Hamad as example).

Study Area

The Wadi Hamad area represents part of the North Eastern Desert of Egypt. This area is located at about 80 km west of Hurgada city, and bounded by latitudes 27° 2' and 27° 23' N and longitudes 32° 57' and 33° 10' E, covering about 700 km² (Fig. 1).

2. Materials and Methods

In this research various datasets were used, including geological maps, field survey and in-situ sampling to validate the satellite data (Landsat 8 data, ASTER). These datasets were put through various methodological processes, including digital image processing, GIS analysis, field sampling and laboratory examination (Fig.2). In this research ASTER L1B data was used, which was acquired on

April 29, 2001. The remotely sensed data were atmospherically corrected for proper analysis and the methods used for data analysis of Landsat 8 and

ASTER data are band combination, (PCA) and band rationing.

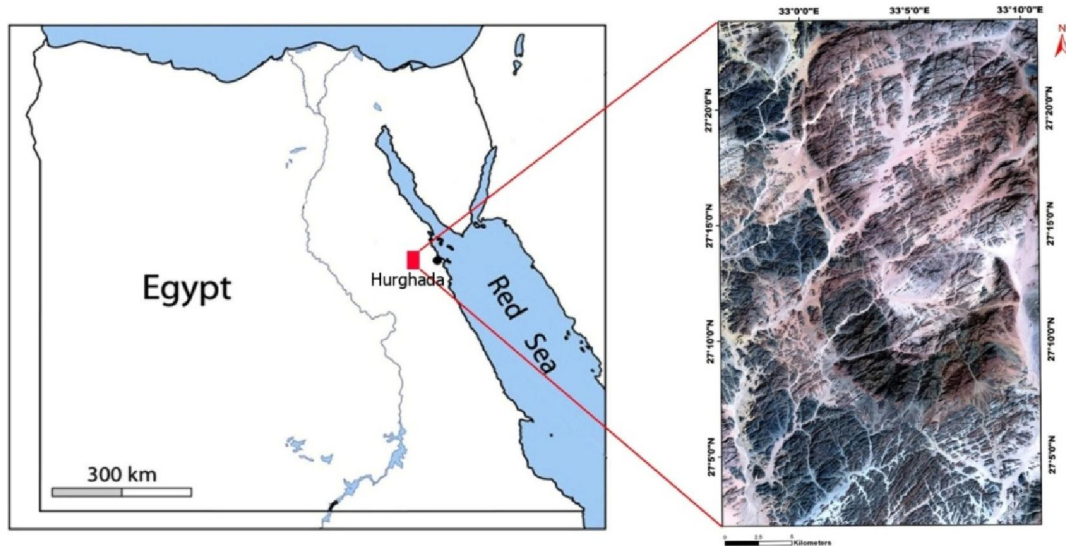


Fig.1. Location map of the Wadi Hamad area, North Eastern Desert.

By using red, green and blue (RGB) color composite images with band combinations it is possible to construct images that differentiate some surface materials based on color variation. Principal Component Analysis (PCA) is used to produce uncorrelated bands as well as to reduce noise and the dimensionality of huge datasets. Band rationing is a digital image processing technique used to effectively display spectral variations (Vincent et al. 1972; Goetz et al. 1975). It is frequently used to reduce the variable effects of solar illumination and topography and enhance spectral information in the image (Holben and Justice 1981). The Optimum Index Factor (OIF) can be used to find the band ratio RGB composite containing the most information by using standard deviation and correlation coefficients (Chavez et al., 1980).

The spectral band-passes of the SWIR bands were found useful in surface mineralogical mapping (Yamaguchi and Naito 2003) and the TIR bands are effective in characterizing the emissivity of the rocks, which consequently used for mapping the silicate rocks (Yamaguchi et al. 1998), so new band ratios are developed to characterize the lithological units of the study area, based on unifying the nominator in band 4 in the NIR spectrum and extends the denominator in a wide range of reflectance in the SWIR and TIR spectrum. The thematic maps were digitized and converted to GIS format for geographic analysis. The digital image processing was carried out using ENVI 5.1 package; however the GIS analysis was carried out using Arc GIS 10.2 package.

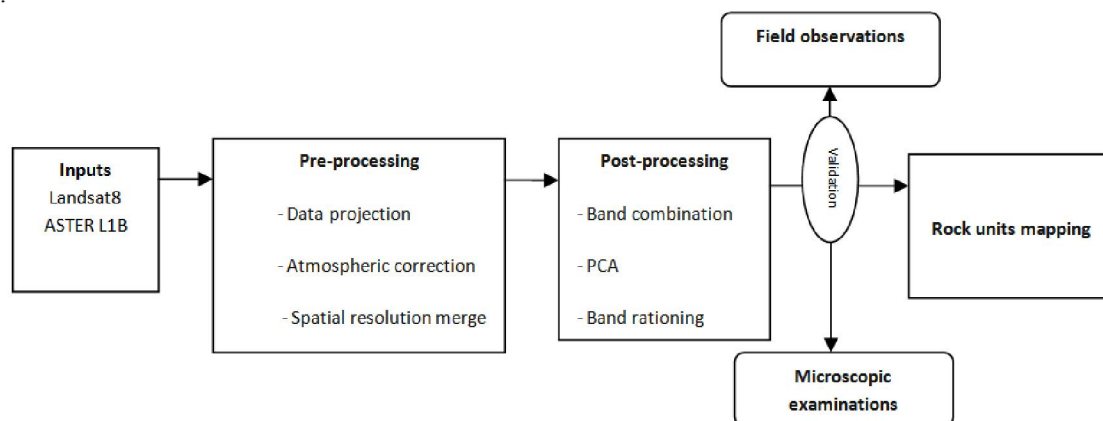


Fig.2. Flowchart of the methodology.

3. Results and Discussion

Visual interpretation of the Landsat 8 and ASTER images was an important step towards understanding the area of study and prepare for the field survey. Landsat 8 band combination 7-3-2 (Fig. 3a) and ASTER band combination 7-3-1 which used as equivalent to Landsat ETM 7-4-2 image (Abdeen et al. 2001) (Fig. 3b), these false color composite images were helpful in the discrimination of granitic rocks from the other rock units in the study area. Not many details on the different lithologic units in the study area can be identified from this image.

Six PCA bands were constructed from Landsat 8 image and Nine PCA bands from ASTER image including VNIR and SWIR. The first PCA band contains the largest percentage of data variance and the second PCA band contains the second largest data variance, and so on; the last PCA bands appear noisy because they contain very little variance, much of which is due to noise in the original spectral data.

The best PCs were determined by analyzing the corresponding eigenvector loadings and the applicability for enhancing different rock types. From the output PCA 6-bands Landsat 8 image we selected three bands (PC6, PC2 and PC1) (Fig.4a) and from 9-bands ASTER image we selected (PC4, PC2 and PC1) (Fig.4b) and According to Amer et al. (2010), the common PC1, PC2 and PC3 were not the best combination to distinguish different lithological units in the central Eastern Desert and (PC5, PC4, and PC2) (Fig.4c) is better to discriminate between ophiolitic rocks. The best RGB composites for visualizing the lithological discrimination using the computed PC bands turned out to be (PC4, PC2 and PC1) for better discriminate Granophyre as dark blue, Dokhan Volcanic – Hammamat Sediments as light blue, Biotite granodiorite as reddish blue from granite.

However, because of their proven ability to enhance compositional variation while suppressing other types of information such as differences in albedo and topographic slope, band ratios are widely used for lithological mapping (Mustard and Sunshine 1998). Therefore, similar to Landsat TM and ETM, ASTER band-ratio combinations and band math are effective in emphasizing spectral characteristics of certain rocks and minerals and hence are more effective in lithological mapping compared to the RGB band combination images (Okada and Ishii 1993; Hewson et al. 2001).

Band ratios (4/7, 3/4, 2/1) ASTER image (Fig. 5a) which is equivalent to (5/7, 4/5, 3/1) Landsat TM image (Abram's combination) used by Abdeen et al. (2001) for mapping serpentinite, granite and marble lithologic units of the Neoproterozoic Allaqi Suture in the southern Eastern Desert of Egypt. Gad and Raef

(2012) used the specific variances and factor loadings of all 72 possible spectral band ratios of visible and near-infrared (VNIR) and shortwave infrared (SWIR) of ASTER data from Wadi Kid in Sinai, Egypt, to construct the best band ratio combinations for lithological mapping. Based on the thereby gained knowledge (6/3, 1/3, 9/5) band ratio combinations were created (Fig. 5b).

Recently ASTER band-ratio (4/7, 4/10, 4/11) (Fig. 5c) were used by Mohy et al. (2016) which integrates SWIR and TIR to characterize and map the lithological units in the Fawakhir area Central Eastern Desert, Egypt showed high performance in the mapping and differentiation of the lithological units. Ahmed et al. (2016) used ratio combination (7/5, 4/3, 6/3) (Fig. 5d) of Landsat 8 data which proved very useful in differentiating various lithologies in the Machulu area, Pakistan. The optimal band selection for ratio images depends on 1) the spectral properties of the surface material of interest and its abundance relative to other surface cover types (Sabine 1999), and 2) The Optimum Index Factor (OIF) developed by Chavez et al. (1980), which is a statistical value that can be used to select the optimum combination of three bands in a satellite image with which a color composite image is created and determined by equation (1).

$$OIF = \frac{Std_i + std_j + std_k}{|Cor_{i,j}| + |Cor_{i,k}| + |Cor_{j,k}|} \quad (1)$$

OIF = The optimum combination of three bands.

Std_i = The standard deviation of band i.

|Cor_{i,j}| = The absolute value of the correlation coefficient of band i and band j.

The optimum combination is the one with the highest sum of standard deviations and the least amount of duplication (lowest correlation coefficient). Herein, we introduce a new ASTER band-ratio images; (4/7, 4/8, 4/10) (Fig. 5e) and (4/6, 4/9, 4/11) (Fig. 5f) that has a high optimum index factor (OIF) and indicative spectral features within these bands. Indeed, all the band ratios showing a clear discrimination of nearly most rock type boundaries in the study area. Even if the ratio composite (4/6, 4/9, 4/11) gives a slightly better contrast between the lithological units where granites are well separated from adjacent rocks by dark blue color, Granophyre having pale blue colors, Dokhan Volcanic has reddish brown colors, Hammamat Sediments have pale brown colors, and Biotite granodiorite a light green color. Quartz diorite and Pyroxene diorite are separated by microscopic examinations and field observations.

Compared to the previous maps on the Wadi Hamad area (Khamis, 1995; Ragab, 2001; Hossny, 2006; Khalaf & Ammar, 2000), the remote sensing methods applied to lithological mapping of the present area have more accurately delineated the boundaries of the different rock units. For example the remote sensing methods used in the present study successfully separated the highly silicic granophyres from the essentially chemically similar alkali feldspar granites. Another important outcome is the differentiation between the Dokhan Volcanics from the commonly associated Hammamat Sediments. More than 150 field points and samples of lithological, structural and alteration information were collected over the study area. Information obtained from these samples was organized into a database and analyzed using Arc GIS 10 software that has been also used to generate the final lithological map of the area (Fig. 6) esert.

Rock descriptions

The Wadi Hamad area is covered by Neoproterozoic volcanic rocks, intrusive rocks and Hammamatmolasse sediments.

The Dokhanvolcanics

The volcanic rocks are exposed in the central (Gabal Um Guruf, Fig.7a) and in the northwestern parts of the area. These rocks belong to the Dokhan Volcanics unit of the basement rocks of Egypt.

They represent the oldest unit in the study area, and are intruded by the associating granitoids (Fig.7b), which send off-shoots in these volcanics and enclose them as xenoliths along their contacts.

These volcanics are essentially composed of intermediate volcanic rocks with subordinate mafic and felsic varieties. They comprise lavas and their pyroclastics, which are commonly intercalated with each others. They are ranging from dark grey, through greenish grey and reddish brown to red. The pyroclastics are represented by ignimbrites, agglomerates and tuffs. The ignimbrites are bedded and exposed essentially to the east of Gabal Um Guruf mass. They vary from dark grey to greenish grey in colour. The agglomerates are not common. The tuffs are bedded, commonly alternating with flow sheets.

Petrographically the Dokhan flows are mainly represented by andesites and dacites subordinate amounts of basalts, basaltic andesites and rhyolites. They are generally porphyritic.

The *andesites* are the most abundant rock variety among the lavas of Wadi Hamad area, either amygdaloidal or nonamygdaloidal. The *andesites* are composed of plagioclase and augite phenocrysts embedded in fine-grained groundmass (Fig.7c) of plagioclase, augite, glass, opaques and quartz. The plagioclase prisms form variolitic and pilotaxitic textures. The amygdales have irregular shape and are filled with epidote.

The *dacites* are also abundant among the lavas. They are porphyritic, either amygdaloidal or nonamygdaloidal and composed of plagioclase and sometimes augite phenocrysts embedded in very fine-grained groundmass of plagioclase and quartz (Fig.7d). Opaques, biotite and apatite are accessories. In the amygdaloidal varieties, the amygdales are of variable sizes and shapes (rounded, amoeboid and irregular). These amygdales are generally zoned, being filled with chalcedony along the peripheral parts followed by chlorite at the cores or filled with epidote or quartz.

The *basalts* are highly porphyritic, hypo to holocrystalline composed of plagioclase and augite phenocrysts embedded in fine-grained groundmass of plagioclase, augite and glass. Opaques are accessory minerals. The plagioclase (An% up to 60) occurs as subhedral prisms, some are fresh and twinned, others are highly altered to sericite or saussurite. The augite occurs mainly in the groundmass, but some occur as microphenocrysts which are usually fresh and twinned, oftenly with thin alteration rims of tremolite or chlorite. The opaques (< 10%) occur as subhedral grains distributed throughout the groundmass. The basalts occasionally contain many amygdales, which are filled with calcite and adularia or with chlorite and epidote. Some of the amygdales are zoned, with chlorite along the peripheries and the calcite at the cores.

The *basaltic andesites* are porphyritic composed of plagioclase and augite phenocrysts embedded in fine-grained groundmass of plagioclase, augite and opaques. Quartz, sericite and epidote are secondary.

The *rhyolites* are porphyritic and leucocratic, composed of orthoclase perthite, quartz and albite phenocrysts embedded in crypto to holocrystalline groundmass of quartz, orthoclase, albite and opaques (Fig.7e). The quartz phenocrysts are sometimes embayed by the groundmass constituents.

The *Pyroclastics* are mainly represented by ignimbrites and tuffs together with subordinate agglomerates.

The *ignimbrites* are represented by welded and non-welded varieties.

The *welded (rheomorphic) ignimbrites* show well-developed pre-tectonic foliation and compaction welding (Fig.7f). Flow foliations vary from a few millimeters to a centimeter in width. The rock is composed of lithic and crystal fragments set in glassy groundmass. The lithic fragments are mostly fiamme, have flame-like ends and significantly variable width: length ratios (mostly 1:>20). They show eutaxitic texture. Sometimes, the fiamme and the enclosing matrix are folded and commonly are sinuously curved, especially around lithic and/or crystal fragments, reflecting the effect of compaction. The fiamme have

dacitic composition and commonly are plagioclase-phyric, especially the relatively thick ones. In addition to the fiamme, lithic fragments (basalts and andesites) are found commonly subangular to subround. The crystal fragments are mainly plagioclase, which vary in shape (subrounded to subangular) and size (ash to lapillus).

The *non-welded ignimbrites* are composed of lithic, plagioclase and subordinate quartz fragments set in very fine to fine-grained matrix. The lithic fragments (andesites and dacites) are represented by subangular to rounded volcanic fragments and subordinate amounts of fiamme, which vary in size from coarse ash to lapillus. The fiamme (dacites) are generally shorter and thicker than those of the welded ignimbrite. They are commonly sinuously curved. The plagioclase fragments varies in size from coarse to fine ash or even fine laths, and in shape from prismatic crystals to angular, subangular or subrounded fragments, which are mostly embayed and corroded by the matrix components. The fine-grained matrix is composed of plagioclase quartz and opaque crystal fragments.

The *agglomerates* are composed of volcanic bombs (commonly porphyritic and amygdaloidal andesites, dacites and basalts) with glassy to tuffaceous matrix. The volcanic bombs are rounded to subrounded. The *lapilli tuffs* are composed of crystal (mainly plagioclase and subordinate amounts of quartz and augite) or of lithic (andesites, dacites, basalts and rhyolites) set in glassy or fine-grained matrix. Some lapilli tuffs contain devitrified fiamme fragments. The *coarse ash tuffs* are composed mainly of plagioclase fragments, with subordinate mafic crystal fragments, set in fine-grained matrix of quartz, plagioclase and opaques.

The *Hammamat sediments* are molasse-type sedimentary rocks, exposed in the southwestern part of the study area, between Wadi Um Guruf and Wadi Hamad and cut by Wadi El-Mesdar. They lie conformably above the Dokhan volcanic rocks and are intruded by the granites. They constitute a relatively thick sequence (up to 150 meters (Fig.7g)), composed of alternating beds of conglomerate, greywacke, siltstone and mudstone (Fig.7h). They vary in colour from greenish grey (conglomerates and greywackes) to brick red (siltstones and mudstones). The conglomerate and greywackes are more common and thicker than the mudstones and siltstones, which show well developed lamination. The Hammamat Sediments are represented by conglomerate, the conglomerates are composed of cobbles of rock fragments (granite, andesite, rhyolite) embedded fine grained matrix (quartz, epidote and plagioclase). The grey wackes are interbedded with siltstone and mudstone. The greywackes are coarse-grained, composed of a high

percentage of clasts and small amount of matrix. The clasts are represented by rock fragments (granite, andesite, rhyolite, and the crystal fragments are of quartz, epidote and plagioclase). The granite clasts are more common, composed of quartz, orthoclase and plagioclase. Some of the granite clasts contain big anhedral crystals of microcline perthites. The andesitic clasts are smaller in sizes and few in number composed of plagioclase laths, quartz and sericite. The plagioclase laths are oriented with their long axes parallel to each other forming a pilotaxitic texture. Some of the andesitic clasts show varulitic texture, hypocrySTALLINE composed of plagioclase laths in glassy groundmass, which contain a high percentage of opaques ~ 15%. The rhyolite clasts are porphyritic, composed of quartz phenocrysts in fine-grained groundmass of quartz, orthoclase, and sericite.

The plagioclase phenocrysts are embayed and corroded by groundmass components. Some of the rhyolite clasts are big and highly amygdaloidal composed of plagioclase phenocrysts of variable sizes embedded in glassy groundmass. The amygdales are filled with epidote. The quartz and orthoclase are aggregated to a mosaic texture possibly due to thermal metamorphism. The quartz clasts are dominantly represented by anhedral grains of variable sizes and subangular boundaries. The matrix is composed of quartz, sericite and clay minerals. The greywacke-siltstone rock is composed of alternate bands of greywacke and siltstone, the latter occurs as thin bands and laminae.

The greywacke bands are much thicker and composed mainly of crystal clasts (quartz, orthoclase, epidote and opaques), together with subordinate amounts of andesite clasts which are either porphyritic or non porphyritic. The quartz clasts are subangular with sharp boundaries. The siltstone composed of quartz clasts in an iron oxide matrix. The bedded siltstone-mudstone rock is composed of alternate bands of siltstone and mudstone. The siltstone bands are composed of fine-grained quartz and plagioclase in a very fine-grained matrix. The quartz show hazy outlines due to the reaction with the matrix components. The plagioclases clasts are extensively sericitized. The mud stones are similar in composition to the siltstone but much finer in the grain size. Sometime the mudstone occurs as thin laminae.

The *intrusive rocks* comprise gabbro, diorites, granodiorites, granophyre and granites. The gabbro is an unmapable mass forming roof-pendants in the granites to the east of the upper reaches of Wadi Um Guruf. This rock is dark grey in colour, coarse-grained, ortho- to adcumulate rock, composed of plagioclase (cumulus phase) and oxyhornblende (intercumulus phase) together with accessory amounts of quartz, opaques and apatite. The oxyhornblende

(brown color) occurs as big anhedral plates, containing subhedral prisms of cumulus plagioclase, in some parts the plagioclase crystals become big due to the adcumulus growth. The plagioclase crystals are usually highly kaolinized.

The diorites are represented by two types, namely pyroxene and quartz diorites. The pyroxene diorites crop out along the western bank of Wadi Um Tweir in the northwestern part of the study area (Fig.8a). They form a moderate topography of small intrusions cutting the Dokhan volcanic rocks. The pyroxene diorites range in size from coarse-grained to pegmatitic, and in colour from dark grey to light greenish grey. They are hypidiomorphic granular rocks, composed of plagioclase and diallage together with accessory amounts of opaques, quartz and apatite. The diallage rocks second in abundances and occur as big fresh anhedral equant crystals and short prisms.

The quartz diorites are exposed along the southern part of Wadi Hamad and extend westwards outside the study area. They form low to moderate relief hills, which are intruded by the granites and contain numerous volcanic xenoliths along the contact with Dokhan volcanic rocks. These rocks are generally equigranular, medium to coarse-grained, mesocratic and greenish to whitish green in colour. Sometimes, these rocks are sheared. These rocks show hypidiomorphic granular texture in the least sheared parts. They are composed of plagioclase, quartz and biotite (Fig.8b). Opaques and sphene are accessories, epidote is secondary. The plagioclase is a predominant constituent, occurs as subhedral to anhedral fresh prisms. The quartz occurs as anhedral grains, occupying the interstitial spaces between the plagioclase. The biotite occurs as subhedral to anhedral flakes in the interstitial spaces between the plagioclase and the quartz. **The granodiorites** are represented essentially by biotite granodiorite and subordinate porphyritic granodiorite. The biotite granodiorite crops out in the southern part of the area, as big pluton which extends outside the mapped area. This pluton is intruding the Dokhan-Hammamatvolcanosedimentary succession and intruded by granites.

It is extensively weathered forming low hills (Fig.8c), which are cut by essentially NE trending dyke swarms. The biotite granodiorites are grey to whitish grey in colour and exfoliated. The porphyritic granodiorite is exposed as a small mass intruding into the Dokhan volcanic rocks to the north of the biotite granodiorite pluton. They are medium to coarse-grained and stained red. The biotite granodiorite are coarse-grained, hypidiomorphic granular rocks, composed of plagioclase, orthoclase perthites, biotite, hornblende and quartz (Fig.8d). Opaques, apatite and sphene are accessories. The plagioclase is the

dominant among the feldspars, occurring as subhedral to anhedral fresh prisms. The orthoclase perthites occur as big anhedral crystals, occupying the interstitial spaces between the plagioclase. The biotite occur as anhedral flakes and tabular crystals, interstitial towards the feldspar. The hornblende (green color) occurs as anhedral short prisms and cross sections, strongly pleochroic, X= yellow, Y= green, Z = brownish green. The porphyritic rocks, composed of plagioclase phenocrysts in medium grained-groundmass of plagioclase, quartz and biotite. Opaques are accessory.

The granophyres are exposed in the middle part of the Wadi Hamad area as moderate relief hills (El Hamara and Khashm El Risha). They are intruding the Dokhan volcanic rocks, (Fig.8e) taking them as large roof-pendants. They are red-coloured medium-grained rocks.. The granophyres are porphyritic, composed of plagioclase phenocrysts and orthoclase microphenocrysts, set in a medium-grained ground mass of quartz, orthoclase, opaques and biotite. Epidote is secondary. The plagioclase phenocrysts are big stout prisms, usually fresh and twinned. The quartz is intergrown with the orthoclase forming the micrographic intergrowths (Fig.8f). The quartz occurs also as small anhedral microphenocrysts. The orthoclase microphenocrysts occur as rectangular crystals. The graphic intergrowths are mainly in the groundmass surrounding the plagioclase microphenocrysts and the quartz and the orthoclase phenocrysts. The biotite flakes are small in size and enclosed in the graphic groundmass. **The granites** cover vast areas, forming moderate to high relief hills. They are represented by biotite - and alkali-feldspar granites. **The biotite granite** is of limited distribution (unmapable), cropping along the northern margin of the biotite granodiorite pluton, suggesting a possible genetic relationship. The biotite granite is medium to coarse-grained and pinkish grey in colour. These are coarse-grained, allotriomorphic granular rocks, composed of orthoclase perthite, plagioclase, quartz and biotite. Opaques, sphene and apatite are accessories. The orthoclase perthite (string perthites) occurs as big anhedral grains, containing small plagioclase prisms as inclusions. The plagioclase occurs as big stout prisms with sericitized cores. The quartz occurs as big anhedral grains, occupying the interstitial spaces between plagioclases. The biotite occurs as anhedral flakes and short prisms in the interstitial spaces between the feldspars and the quartz.

The alkali-feldspar granites are the predominant among the granites, intruding all the previously mentioned rocks. The main mass of the alkali-feldspar granites occupies the northern part of the mapped area as high relief hills (Fig.8g) and is traversed by Wadi Hamad and Wadi Abu Harba.

Smaller intrusions are exposed in the southwestern part of Wadi Hamad area. The alkali-feldspar granites are pink in colour and coarse-grained leucocratic rocks. These are coarse-grained allotriomorphic granular rocks, composed of albite, orthoclase perthites (Fig.8h) and quartz. Biotite, opaques, sphene and muscovite are accessories. The albite (> 30% by volume) occurs as subhedral and anhedral prisms, which are usually fresh and twinned. The orthoclase

perthites (string type) rank second in abundance, occurs as big anhedral crystals, occupying the interstitial spaces between albite and corroding and enclosing albite as inclusions. The quartz occurs as anhedral crystals occupying the interstitial spaces and corroding the feldspars. The biotite and muscovite flakes are tabular crystals (up to 5% by volume) varying in the amount from sample to another.

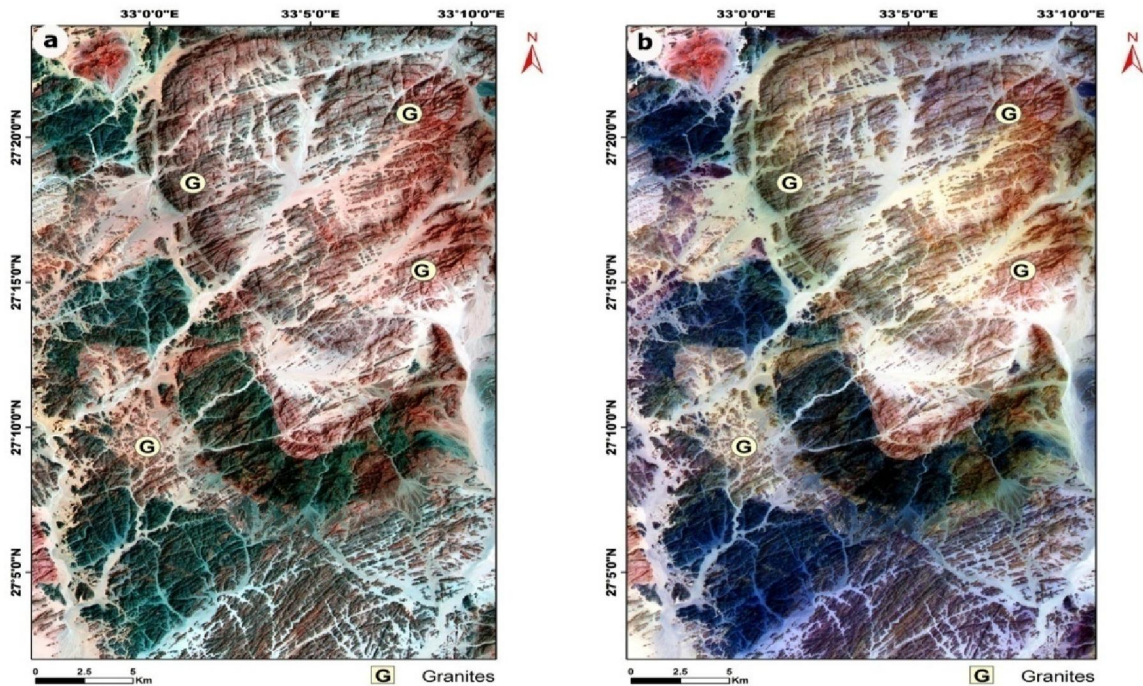


Fig.3 (a) Landsat 8 false color composite of 7-3-2 (b) ASTER false color composite of 7-3-1

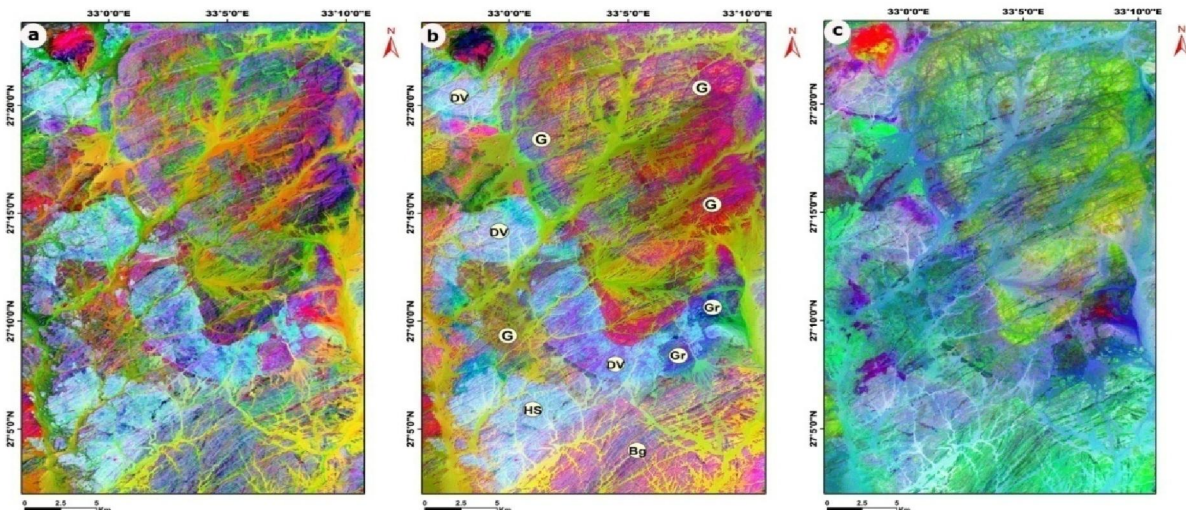


Fig. 4. Principal Component Analysis (PCA) (a) PC6, PC2, PC1 (b) PC4, PC2, PC1 (c) PC5, PC4, PC2. {G} Granite – {Gr} Granophyre – {DV} Dokhan Volcanic – {HS} Hammamat Sediments – {Bg} Biotite granodiorite

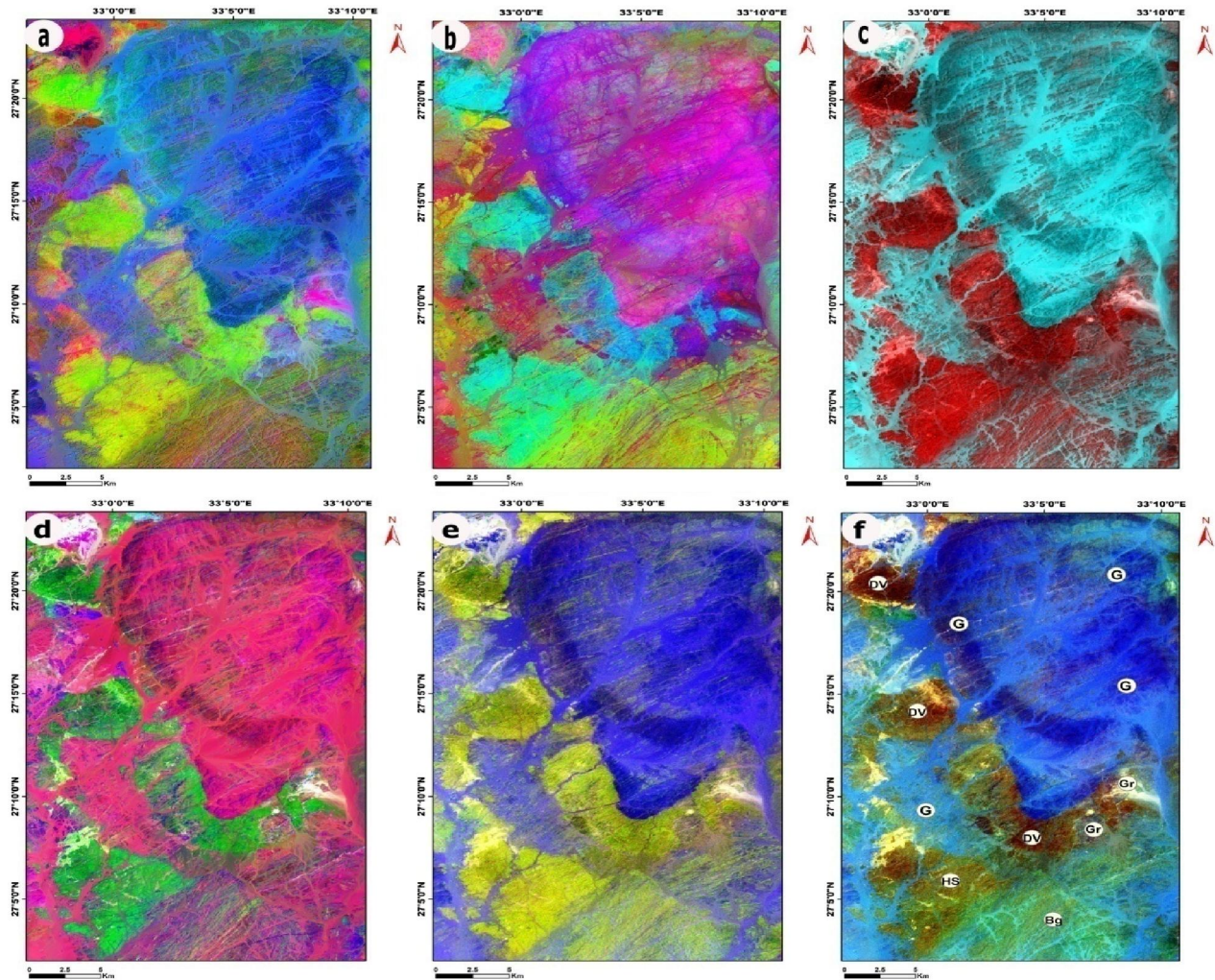


Fig. 5. Band ratios created by considering OIF ranking, and band ratios mentioned in publications.

(a) 4/7-3/4-2/1 (Abdeen et al.2001) (b) 6/3-1/3-9/5 (Gad & Raef 2012)

(c) 4/7-4/10-4/11 (Mohy et al.2016) (d) (7/5, 4/3, 6/3) Ahmed et al. (2016)

(e) 4/7-4/8-4/10 (high OIF) (f) 4/6-4/9-4/11 (high OIF)

{G} Granite – {Gr}Granophyre – {DV} Dokhan Volcanic – {HS} Hammamat Sediments – {Bg} Biotite granodiorite

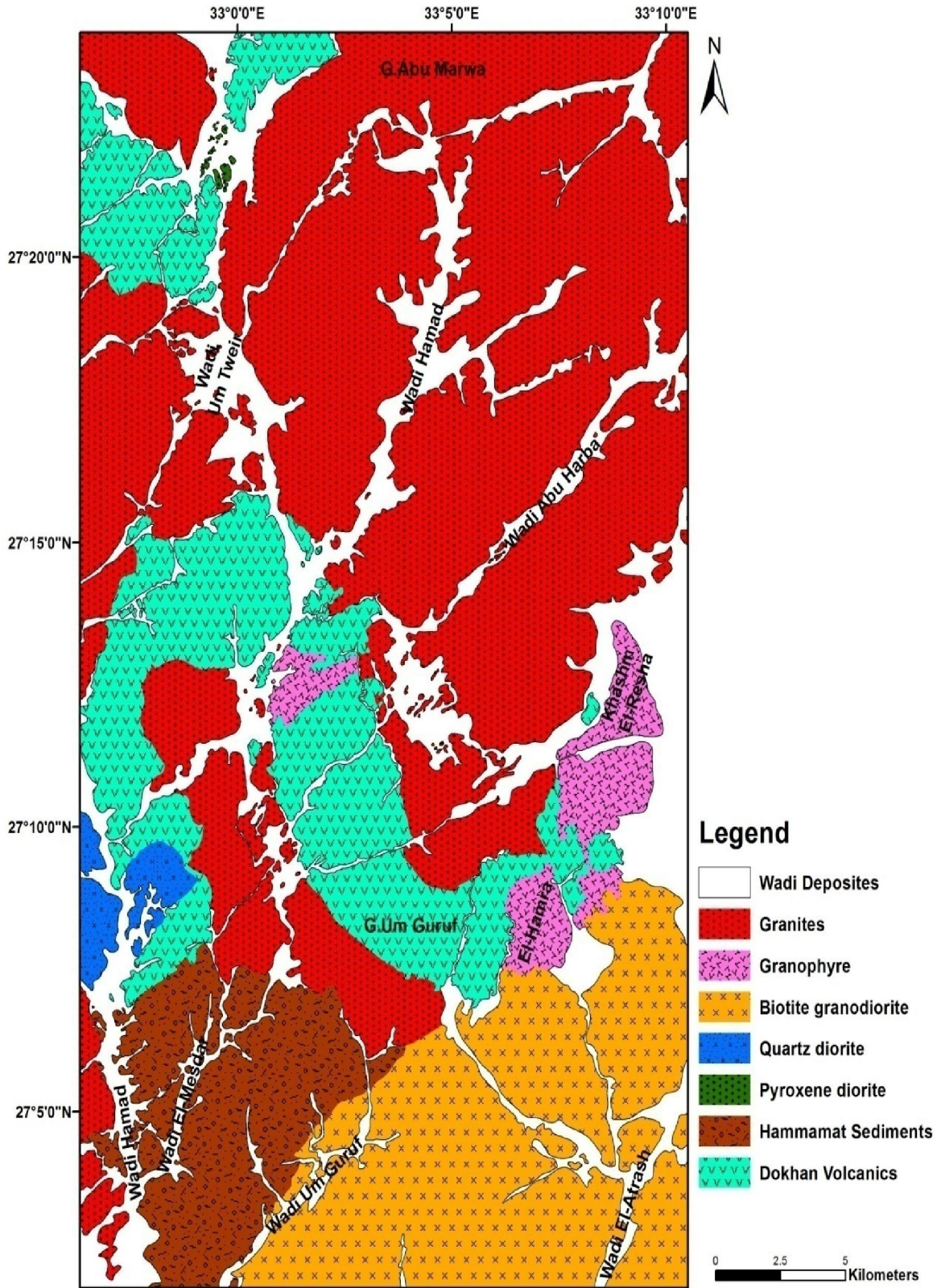


Fig. 6. Final lithological map of the Wadi Hamad area, North Eastern D

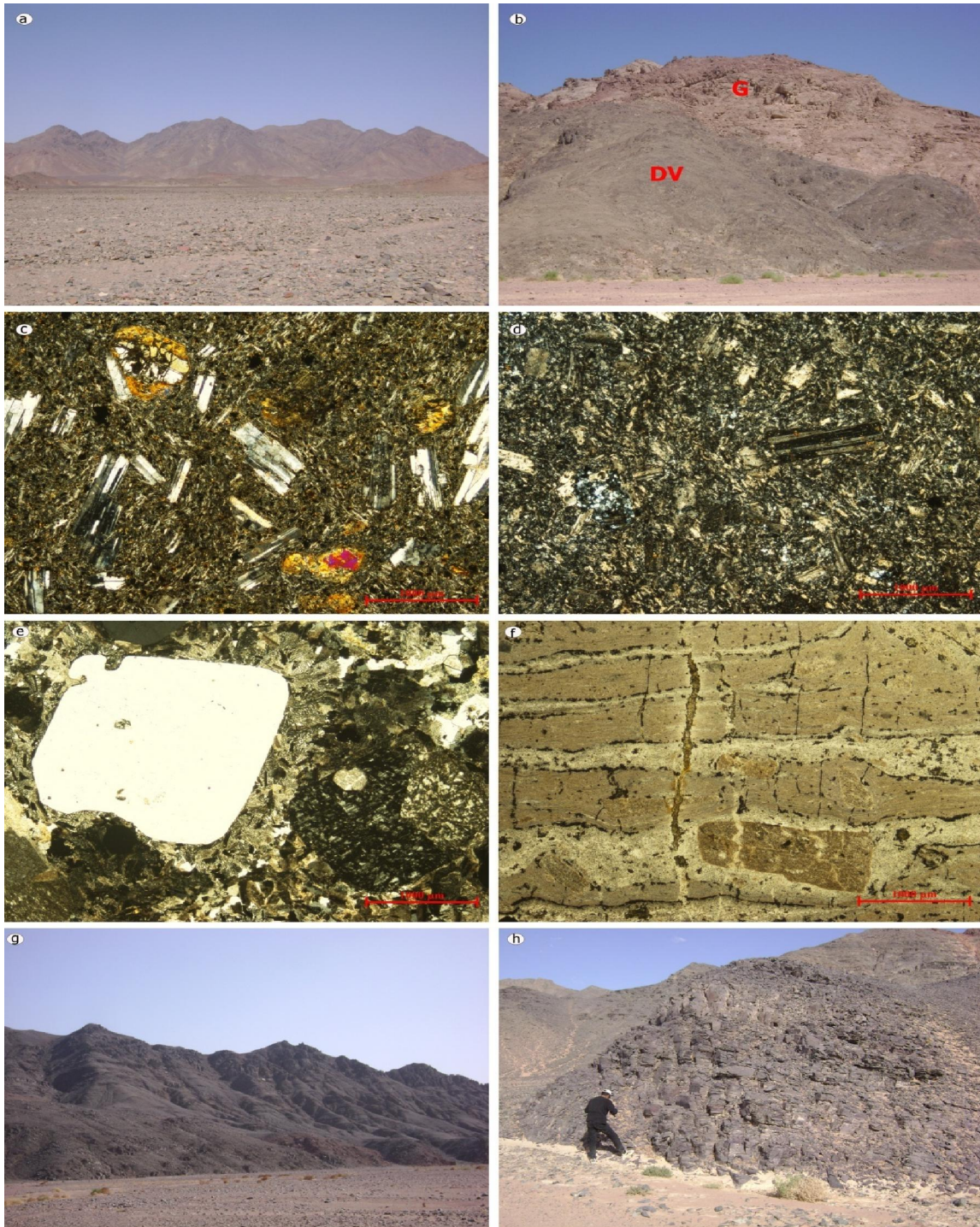


Fig.7 Field and petrographic characteristics of Dokhan Volcanics and Hammamat Sediments of Wadi Hamad area. (a) General view showing Gabal Um Guruf volcanics. (b) Granites {G} intruding the Dokhan Volcanics {DV} (c) Photomicrograph for the porphyritic andesite showing plagioclase and clinopyroxene phenocrysts in fine-grained groundmass, CN. (d) Photomicrograph for the dacite showing plagioclase phenocryst and microcrystalline quartz-filled amygdale in fine-grained groundmass, CN. (e) Photomicrograph for the rhyolite showing quartz and perthite phenocrysts in microcrystalline groundmass, CN. (f) Photomicrograph for the welded ignimbrite showing well-developed pre-tectonic foliation and compaction welding, PL. (g) General view for the Hammamat Sediments succession. (h) Field photo showing bedded Hammamat siltstone.

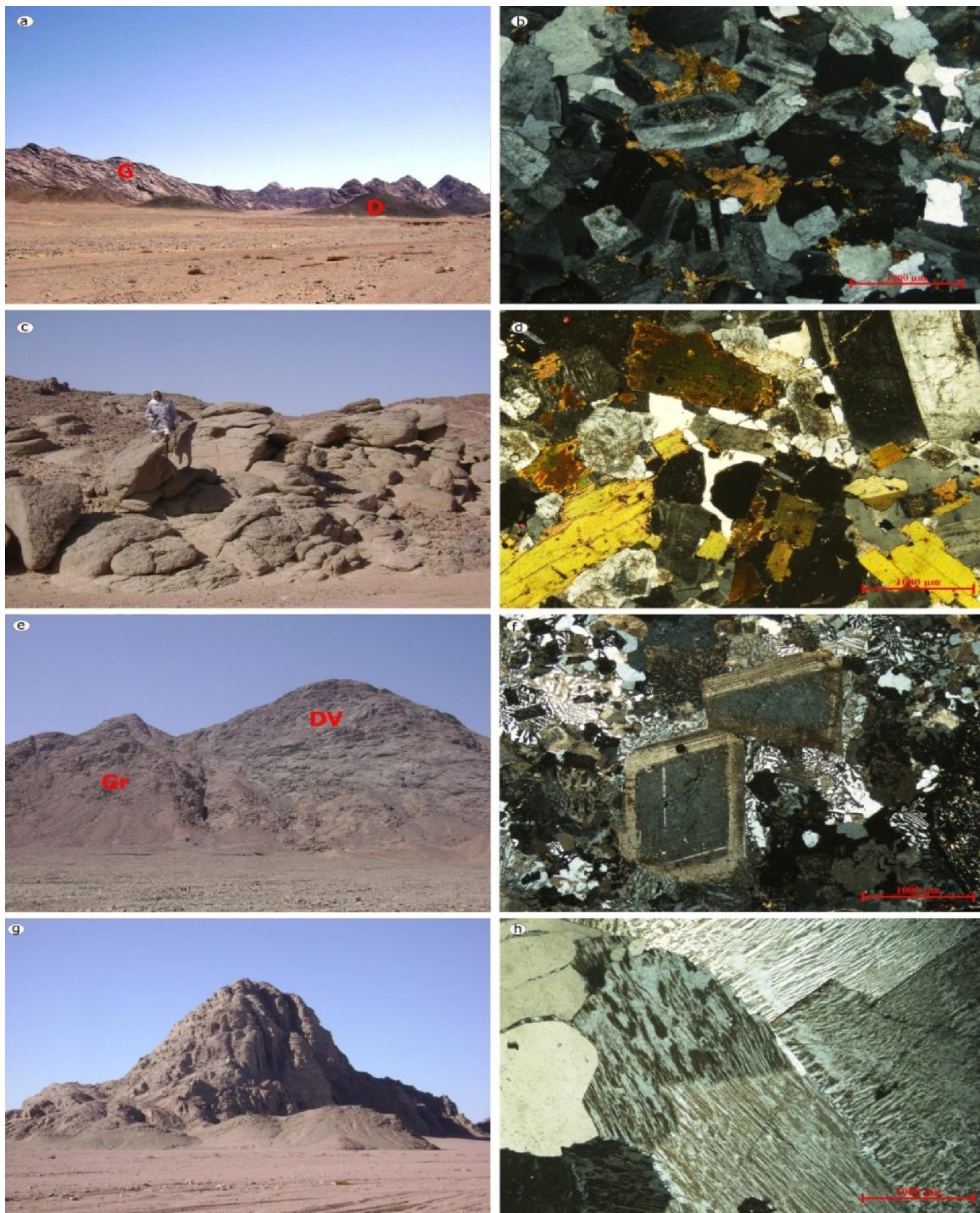


Fig.8 Field and petrographic characteristics of the intrusive rocks of Wadi Hamad area.

(a) Field photo showing low-laying pyroxene diorite {D} in the foreground and granites {G} in the background. (b) Photomicrograph for the quartz diorite showing hypidiomorphic granular texture, CN. (c) Field photo showing highly weathered low-laying granodiorite. (d) Photomicrograph for the biotite granodiorite, showing hypidiomorphic granular texture, CN. (e) Granophyre {Gr} intruded into the Dokhan Volcanics {DV}, G. El-Hamra (f) Photomicrograph for the granophyre showing plagioclase phenocrysts and micrographic texture, CN. (g) Field photo of the high topography of the alkali feldspar granite along Wadi Abu Harba. (h) Photomicrograph for the Alkali feldspar granite showing allotriomorphic granular and perthitic textures, CN.

Conclusions

Lithological mapping is an important issue for understanding the mineralogy and the geology of Egypt (arid and exposed area). Using Landsat 8 and ASTER data enables us to discriminate at least the main lithological units in the Wadi Hamad area. The approach of using OIF for the determination of study area specific ratios achieved promising results, giving a good contrast and discriminability of occurring rock types.

The conventional methods are time, effort and budget wasting that are difficult to use in developing countries like Egypt. The earth observation techniques enable such lithological mapping, however new methodologies and approaches are under further development. It is more apparent that coupling Landsat 8 and ASTER data with decent areal coverage and other field knowledge is powerful for detailed lithological mapping. The final lithological map was validated against field studies and previously published geologic maps.

References

1. Abdeen, M.M., Allison, T.K., Abdelsalam, M.G., Stern, R.J. (2001) Application of ASTER band-ratio images for geological mapping in arid regions; the Neoproterozoic Allaqi Suture, Egypt. Abstract with Program Geol. Soc. America, vol. 3(3), p. 289.
2. Ahmed, L., Shah, M.Tahir., D.Khan, Shuhab (2016) Reflectance spectroscopy and remote sensing data for findingsulfide-bearing alteration zones and mapping geologyin Gilgit-Baltistan, Pakistan. *Earth Sci Inform* (9):113–121.
3. Amer, R.M., Kusky, T.M., Ghulam, A. (2010) Lithological mapping in the Central Eastern Desert of Egypt using ASTER data. *J. Afri. Earth Sci.* 56, 75–82.
4. Chavez, P.S., Berlin, G.L., Sowers, L.B. (1980) Statistical methods for selecting of Landsat MSS ratios. *Journal of Applied Photographic Engineering* 8, 30–32.
5. Fritz, H., Abdelsalam, M., Ali, K.A., Bingen, B., Collins, A.S., Fowler, A.R., Ghebreab, W., Hauzenberger, C.A., Johnson, P.R., Kusky, T.M., Macey, P., Muhongo, S., Stern, R.J., Viola, G. (2013) Orogen styles in the East African Orogen: A review of the Neoproterozoic to Cambrian tectonic evolution. *Journal of African Earth Sciences* 86, 65-106.
6. Genna, A., Nehlig, P., Le Goff, E., Gguerrot, C., Shanti, M. (2002) Proterozoic tectonism of the Arabian Shield. *Precambrian Research* 117, 21-40.
7. Gad, S., Raef, A. (2012) Factor analysis approach for composited ASTER band ratios and wavelet transform pixel-level image fusion: lithological mapping of the Neoproterozoic Wadi Kid area, Sinai, Egypt. *Int. J. Remote Sens.* 33 (5), 1488e1506.
8. Goetz F.H., Billingsley F.C., Gillespie AR., Abrams MJ., Squires R L., Shoemaker E M. Lucchitta I and Elston D P (1975) Application of ERTS images and image processing to regional problems and geological mapping in northern Arizona, JPL Technical Report 32–1597.
9. Hewson, R., Cudahy, T. and Huntington, J. (2001) Geologic and alteration mapping at Mt Fitton, south Australia, using ASTER satellite-borne data. *Geoscience and Remote Sensing Symposium*, 2: 724-726.
10. Holben BN, Justice CO (1981) An examination of spectral band ratioing to reduce the topographic effect on remotely sensed data. *Int J Remote Sensing* 2(2):115–133.
11. Hossny, H.A.H. (2008) Geochemistry, petrogenesis and geochemical exploration of the rock association at Wadi Hammad District, north Eastern Desert, Egypt. Ph D thesis, Faculty of Science, Alexandria University.
12. Khalaf, A.E., Ammar, F. (2000) Late Proterozoic igneous complex from Umm Guruf area, North Eastern Desert, Egypt: Implication for open system fractional crystallization. 5th International Conference of the Arab World, Cairo University, Egypt, p. 89-112.
13. Khamis, H. A. (1995) Radioactivity and structure of Wadi Hammad area, North Eastern Desert, Egypt. Msc Thesis, Cairo University, Faculty of Science, Egypt, p235.
14. Mohy, H., Abou El-Magd, I., Basta. F (2016) Newly Improved Band Ratio of ASTER Data for Lithological Mapping of the Fawakhir Area, Central Eastern Desert, Egypt. *Journal of the Indian Society of Remote Sensing* 44 (5), 735-746.
15. Mustard, J.F., Sunshine, M.J. (1998) Spectral analysis for earth science: investigations using remote sensing data, In: Rencz, Andrew (ed.), 3rd ed. *Remote Sensing for the Earth Sciences: Manual for Remote Sensing*, 3: 251–306.
16. Okada, K., Ishii, M. (1993) Mineral and lithological mapping using thermal infrared remotely sensed data from ASTER simulator. *Int. Geosci. and Remote Sensing Symposium “Better Understanding of Earth Environment”*, 93: 126–128.
17. Ragab, A.A.A. (2001) Mineralogical, geochemical and radioactive studies of Wadi

- Abu Hamad-Wadi El-Atrash area, Northern Eastern Desert, Egypt. Ph D, Faculty of Science, Ain Shams University, 314p.
18. Sabine, C. (1999) Remote sensing strategies for mineral exploration. In: A. Rencz (ed.), *Remote Sensing for the Earth Sciences-Manual of Remote Sensing*. New York: Am. Soc. Photogrammetry and Remote Sensing/John Wiley and Sons: 375-447.
 19. Stern, R.J. (1994) Arc assembly and continental collision in the Neoproterozoic East African Orogen: implications for the consolidation of Gondwanaland. *Annual Reviews of Earth and Planetary Science* 22, 319-351.
 20. Stern, R.J., Hedge, C.E. (1985) Geochronological and isotopic constraints on Late Precambrian crustal evolution in the Eastern Desert of Egypt. *American Journal of Science* 285, 97-127.
 21. Vincent RK, Thomson F, Watson K (1972) Recognition of exposed quartz sand and sandstone by two-channel infrared imagery. *J Geophys Res* 77:2473-2477.
 22. Yamaguchi, Y., Kahle, A.B., Kawakami, T., Paniel, M. (1998) Overview of the advanced spaceborne thermal emission and reflection radiometer (ASTER). *IEEE Transaction on Geoscience and Remote Sensing* 36 (4): 1062-1071.
 23. Yamaguchi, Y., Naito, C. (2003) Spectral indices for lithologic discrimination and mapping by using the ASTER SWIR bands. *Int. J. Remote Sensing* 24 (22): 4311-4323.

6/21/2017